OBSERVATION OF NUCLEAR-ACOUSTIC-RESONANCE DISPERSION*

R. L. Melcher† and D. I. Bolef
Arthur Holly Compton Laboratory of Physics, Washington University, Saint Louis, Missouri
(Received 25 April 1968)

Observation of the nuclear-acoustic-resonance dispersion mode of F^{19} in antiferromagnetic $RbMnF_3$ is reported. Saturation studies indicate that the dispersion mode saturates at higher ultrasonic powers than does the pure absorption mode.

The purpose of this Letter is to report the observation of the nuclear-acoustic-resonance (NAR) dispersion mode, i.e., the resonant shift in the phase velocity of an ultrasonic wave, due to its interaction with a nuclear spin system. Previous NAR experiments have dealt only with the absorption mode.[1,2] They were designed to detect either the resonant increase in the ultrasonic attenuation or the decrease in nuclear magnetization due to partial acoustic saturation of the nuclear-spin energy levels, both effects arising from coupling of the acoustic phonons to the nuclear spin system. In the present experiment, the NAR dispersion and absorption of 30-MHz longitudinal acoustic waves by the F^{19} nuclei in a single-crystal specimen of antiferromagnetic $RbMnF_3$ were observed by means of a cw transmission ultrasonic spectrometer.[3]

In operation, the carrier frequency ω of the spectrometer rf oscillator is adjusted to the vicinity of a mechanical resonance at frequency ω_n characteristic of the composite acoustic resonator consisting of the sample and two quartz transducers. By precise adjustment of ω relative to ω_n the spectrometer can be made sensitive to either pure absorption or a mixture of dispersion and absorption. The signal at the output of the spectrometer relative to a calibrator signal, when $\omega=\omega_n$ and when magnetic field modulation is used, can be shown to be given by[3]

$$S=-\frac{2}{\alpha_0}\frac{\partial\Delta\alpha}{\partial\omega_0}\Delta\omega_0, \tag{1}$$

where α_0 is the ultrasonic attenuation in the absence of NAR and is equal to the half-width at the half-power point of the mechanical resonance; $\Delta\alpha=\alpha-\alpha_0$ is the change in the ultrasonic attenuation due to NAR absorption; $\omega_0=\gamma_N H_0$ and $\Delta\omega_0=\gamma_N\Delta H_0$, where H_0 and ΔH_0 are, respectively, the applied dc magnetic field and the amplitude of the audio modulation field. γ_N is the nuclear gyromagnetic ratio. When the carrier frequency ω is tuned to the half-power points on the mechanical resonance, i.e., $\omega-\omega_n=\pm\alpha_0$, the signal is given by

$$S=-\frac{1}{\alpha_0}\left[\frac{\partial}{\partial\omega_0}(\Delta\alpha\mp\Delta\omega_n)\right]\Delta\omega_0, \tag{2}$$

where $\Delta\omega_n$ is the shift in the mechanical resonance frequency resulting from the dispersion of the phase velocity v of the ultrasonic wave at nuclear resonance. The dispersion of the phase velocity is given by $\Delta V=V_0\Delta\omega_n/\omega_n$. V_0 is the phase velocity in absence of NAR dispersion. When frequency modulation is used instead of magnetic field modulation, the expression for the signal differs from that given in Eq. (2).[3]

In Fig. 1 are shown three recorder traces of the first derivative NAR signal obtained in antiferromagnetic $RbMnF_3{}^{19}$ at $T=57.3$°K using magnetic field modulation of 8 Oe peak-to-peak. The

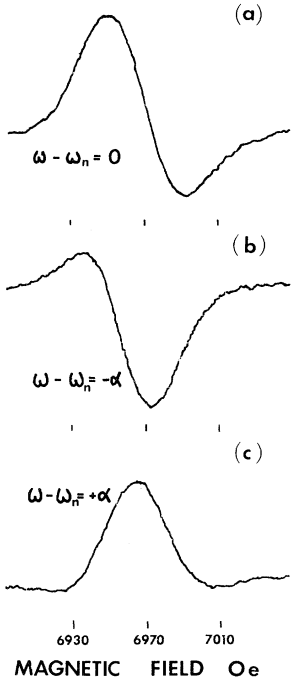

FIG. 1. Recorder traces of the NAR signal observed in $RbMnF_3$ at 57.3°K: (a) $\omega-\omega_n=0$, (b) $\omega-\omega_n=-\alpha_0$, and (c) $\omega-\omega_n=+\alpha_0$. Data taken with 29.67-MHz longitudinal acoustic waves propagating along the [110] axis. The magnetic field was oriented along the [111] axis. Magnetic field modulation of 8 Oe peak-to-peak was used.

pure (slightly asymmetric) NAR absorption line obtained when $\omega = \omega_n$ is shown in Fig. 1(a). Figures 1(b) and 1(c) show the mixed-mode signals for $\omega - \omega_n = \mp\alpha_0$, respectively. The data were taken using 29.67-MHz longitudinal acoustic waves propagating along the [110] axis with the magnetic field $\vec{H}_0$ parallel to the [111] axis of the cubic crystal. At this temperature and magnetic field orientation the three F^{19} nuclear sites are equivalent. The line shapes in Figs. 1(b) and 1(c) clearly show the admixture of the dispersion mode into the NAR signal.

Nuclear-spin–acoustic-phonon coupling in antiferromagnetic insulators has been investigated theoretically by Silverstein[4] and by Buishvili and Giorgadze[5] for the case of uniaxial symmetry. Both of these treatments are concerned with coupling mechanisms arising from the interaction with the ordered electronic magnetic moments. The lowest-order phenomenological interaction which one can write involving the elastic strains, the electronic sublattice magnetization, and the nuclear magnetization must be linear in these quantities (we consider nuclei with spin $I = \frac{1}{2}$). Allowing for the cubic symmetry of $RbMnF_3$ one obtains an effective nuclear-spin–acoustic-phonon interaction of the form

$$\epsilon_{\text{int}} = g M_x I_x e_{xx}. \tag{3}$$

In Eq. (3) we have considered only a longitudinal ultrasonic strain e_{xx} with propagation along the x axis. I_x is the x component of the nuclear magnetization, and M_x is the corresponding component of the electronic sublattice magnetization. The phenomenological coupling constant g characterizes the strength of the interaction.

Jacobsen and Stevens[6] have considered a semiclassical approach to the ultrasonic dispersion and absorption due to the interaction of acoustic waves with electron spins in solids. Utilizing a classical approach analogous to theirs and the above phenomenological interaction, one can derive, in the linear approximation, a dispersion relation for the coupled elastic and nuclear magnetic systems. From this dispersion relation one obtains the following expression for the phase velocity of the acoustic wave:

$$v = v_0 - \frac{g^2 M_x^{\,2} \chi_0 \omega_0^{\,2} \tau_N^{\,2}}{2\rho v_0 [1 + (\omega_0^{\,2} - \omega^2)\tau_N^{\,2} + 2i\omega\tau_N]}, \tag{4}$$

where ρ is the density of the sample, χ_0 is the nuclear susceptibility, and τ_N is the nuclear spin-spin relaxation time. We have considered in Eq. (4) only the case for $\vec{H}_0$ perpendicular to the direction of propagation. The real part of $v - v_0$ is the dispersion in the phase velocity due to NAR, while the imaginary part is proportional to the NAR attenuation coefficient $\Delta\alpha$. In the neighborhood of nuclear resonance ($\omega \simeq \omega_0$) the absorptive and dispersive components of $v - v_0$ have the usual resonance shapes.[6]

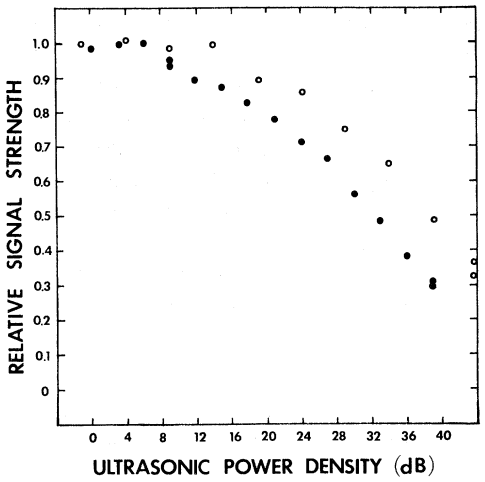

FIG. 2. Saturation measurements of the NAR absorption and the mixed NAR dispersion and absorption. $T = 57.3°K$, $\nu = 29.67$ MHz, $\vec{H}_0 \| [111]$; longitudinal waves propagate parallel to the [110] axis. The solid dots correspond to pure absorption ($\omega = \omega_n$) and the open circles correspond to the mixed dispersion and absorption mode ($\omega - \omega_n = +\alpha_0$).

By comparing the data shown in Fig. 1 with a known calibrator signal, one can calculate the phase velocity dispersion to be $\Delta v/v \simeq 5 \times 10^{-8}$. The corresponding resonant change in the ultrasonic attenuation coefficient is $\Delta\alpha \simeq 4\ \text{sec}^{-1}$. It is of interest to compare the saturation properties of the absorption and the mixed absorption and dispersion modes. Shown in Fig. 2 is the signal strength as a function of ultrasonic power density for the pure absorption (solid dots) and for the mixed (absorption-minus-dispersion) mode. Clearly the pure absorption mode saturates at a lower (~6-dB) power density than the mixed mode. This fact makes the dispersion mode somewhat more useful than absorption when saturation is a factor in NAR studies. The ultrasonic power density at 0 dB in Fig. 2 was approximately $10^{-8}\ \text{W/cm}^2$, corresponding to an energy density ($\epsilon = P/v$) of $10^{-7}\ \text{erg/cm}^3$.

Redfield has treated in detail saturation for the case of conventional NMR in solids.[7] No treat-

ment exists, to our knowledge, of saturation for the case of nuclear acoustic resonance. However, the conclusion of Redfield that the Bloch equations do not apply to solids in the saturation limit certainly holds in the case of nuclear acoustic resonance also. The Bloch equations predict that the dispersion mode would not saturate, contrary to the present results.

We thank Dr. R. W. H. Stevenson for supplying the single-crystal specimens of $RbMnF_3$.

*Research sponsored in part by the Air Force Office of Scienctific Research, Office of Aerospace Research, U. S. Air Force, under AFOSR Grant No. 68-1412.

†National Science Foundation Graduate Fellow.

[1]D. I. Bolef, in Physical Acoustics, edited by W. P. Mason (Academic Press, Inc., New York, 1966), Vol. 4A, Chap. 3.

[2]R. L. Melcher, D. I. Bolef, and R. W. H. Stevenson, Phys. Rev. Letters 20, 453 (1968).

[3]R. L. Melcher, D. I. Bolef, and J. B. Merry, to be published.

[4]S. D. Silverstein, Phys. Rev. 132, 997 (1963).

[5]L. L. Buishvili and N. P. Giorgadze, Fiz. Tverd. Tela 7, 769 (1965) [translation: Soviet Phys. Solid State 7, 614 (1965)].

[6]E. H. Jacobsen and K. W. H. Stevens, Phys. Rev. 129, 2036 (1963).

[7]A. G. Redfield, Phys. Rev. 98, 1787 (1955).

ORIGIN OF THE ANGULAR DEPENDENCE OF SECONDARY EMISSION OF ELECTRONS FROM TUNGSTEN*

R. M. Stern and H. Taub†
Department of Physics, Polytechnic Institute of Brooklyn, Brooklyn, New York
(Received 2 April 1968)

The existence of strong variations in the total secondary electron current with incident beam direction from a tungsten (110) surface can be explained on the basis of the observed angular distribution of the secondary emission and the reciprocity theorem. We propose a dynamical two-beam model based on the variation of electron absorption in the crystal as a function of the diffraction conditions.

There has been much speculation as to the origin of the angular-dependent secondary emission of electrons in crystals.[1-6] Measurements have been made of the secondary emission from tungsten (110) as a function of angle using low-energy electron diffraction (LEED) techniques with primary electron energies between 50 and 2200 eV. Using a commercial LEED system the total current from the crystal to ground can be measured directly and the current from crystal to screen (subtending an angle of 120 deg) can be measured and energy analyzed using the existing grid system.

At low incident energy the diffraction is predominantly elastic. The conservation of current requires that as the incident direction is varied the resulting exchange of total diffracted current between Laue and Bragg reflections is accompanied by variations of the total secondary emission. Other elastic dynamical effects[7-9] in this region also contribute much fine structure to these rocking curves making analysis of the secondary emission at low voltages difficult. Above 1000 eV, where Bragg reflections and multiple-diffraction-associated fine structure appear to be unimportant, the secondary current is predominantly inelastic and the amplitude angular variations of the secondary emission become quite large as shown (at 2000 eV) in Fig. 1.

A definite correlation exists between the position of the structure in rocking curves of this type and the directional dependence of the total secondary emission displayed in the observed Kikuchi pattern, shown in Fig. 2(a) (2000 eV).

Observations of Kikuchi patterns have become quite common in low-energy electron diffraction.[10-14] These patterns have their origin in electrons which scatter incoherently by some as yet unspecified mechanism, and thereafter scatter elastically before leaving the crystal. This, in effect, creates an incoherent internal source[10] of electrons in the crystal. While dynamical theories[15,16] exist which describe the diffracted intensity distribution, the positions of the lines and bands which make up the pattern can be predicted by simple geometrical arguments.[10,13] For tungsten, the Kikuchi pattern, composed of reversing bands, deficiency lines, and the deficiency limiting circles described by Shinohara,[17] is the dominant diffraction feature above 600 eV. Shinohara circles are found about the (110), (111), and (100) type poles and appear to bound